Research Square

Preprints are preliminary reports that have not undergone peer review.
They should not be considered conclusive, used to inform clinical practice,
or referenced by the media as validated information.

Evaluation of Processing Parameters in the Hydrothermal Carbonisation of African Fan Palm Nut

Calistus Princewill Odeh
Nnamdi Azikiwe University Faculty of Engineering
Augustine Uzodinma Madumere
Nnamdi Azikiwe University Faculty of Engineering
John Chikaelo Okeke
jc.okeke@unizik.edu.ng
Nnamdi Azikiwe University Faculty of Engineering https://orcid.org/0009-0005-4879-1053
Henry Chukwuemeka Olisakwe
Nnamdi Azikiwe University Faculty of Engineering
Orobosa Kingsley Osazuwa
Nnamdi Azikiwe University Faculty of Engineering

Research Article

Keywords: Hydrothermal carbonisation (HTC), Hydrochar production, African fan palm nut, Biomass valorization, Sustainable biomass conversion, Porous carbon materials

Posted Date: March 25th, 2026

DOI: https://doi.org/10.21203/rs.3.rs-9012832/v1

License: This work is licensed under a Creative Commons Attribution 4.0 International License.
Read Full License

Evaluation of Processing Parameters in the Hydrothermal Carbonisation of African Fan Palm Nut

[1]Calistus Princewill Odeh, [1]Augustine Uzodinma Madumere, [1]John Chikaelo Okeke*, [1]Henry Chukwuemeka Olisakwe, [1]Orobosa Kingsley Osazuwa

1. Department of Mechanical Engineering, Nnamdi Azikiwe University, Awka, Anambra State, Nigeria

Corresponding author: John Chikaelo Okeke
Email: jc.okeke@unizik.edu.ng

Abstract

This study explores the conversion of African fan palm nut an underutilized agricultural waste into valuable hydrochar using hydrothermal carbonization (HTC). The main aim was to optimize the HTC process conditions and assess the physicochemical characteristics of the produced hydrochar for potential use as an adsorbent. HTC experiments were carried out in a temperature-controlled batch reactor under inert conditions. Process optimization was performed using Response Surface Methodology (RSM) with a Central Composite Design (CCD), considering reaction temperature (180-220 °C), residence time (30-90 min), and biomass-to-water ratio (1:8–1:12). The optimal conditions were determined to be 220 °C, a residence time of 70.22 min, and a biomass-to-water ratio of 1:10.06. At these conditions, hydrochar and bio-oil yields of 24.72% and 28.60%, respectively, were achieved, alongside a maximum specific surface area of 729.56 $m^2 g^{-1}$. The resulting hydrochar exhibited desirable properties, including high carbon content (80.00%), low ash content (0.78%), and well-developed surface characteristics, confirming its suitability for adsorption-based applications. Overall, the results highlight African fan palm nut as a promising and sustainable feedstock for hydrochar production via HTC. This study supports the valorization of biomass waste and contributes to the development of environmentally sustainable materials in line with the Sustainable Development Goals (SDGs). Further studies should focus on application-specific performance, process scalability, and comprehensive environmental sustainability assessments.

Keywords: Hydrothermal carbonisation (HTC), Hydrochar production, African fan palm nut, Biomass valorization, Sustainable biomass conversion, Porous carbon materials

1. Introduction

Hydrothermal carbonization (HTC) has emerged as a promising thermochemical route for converting biomass into value-added carbon-based materials, representing a significant advancement in sustainable materials research. The process is typically conducted in a sealed reactor at temperatures between 180 and 250 °C, where internal pressure develops naturally due to water vapor formation and related reactions [1]. Depending on the nature of the feedstock and the desired product characteristics, residence times commonly vary from 0.5 to 8 h, allowing for the efficient conversion of wet biomass into hydrochar [1]. HTC operates in a subcritical, water-rich environment under relatively mild conditions, facilitating key reactions such as dehydration, decarboxylation, and polymerization. These reactions lead to the formation of hydrochar, a carbon-rich solid with wide-ranging application potential [2, 3]. Compared to conventional thermochemical processes, HTC offers a clear advantage in its ability to

directly process biomass with high moisture content, eliminating the need for energy-intensive drying steps.

One of the key advantages of hydrothermal carbonization is its ability to accommodate a wide variety of biomass feedstocks without requiring energy-intensive pre-drying. The direct processing of wet biomass lowers overall energy consumption and reduces operational costs in biomass conversion systems. Moreover, hydrochars produced through HTC often possess favorable physicochemical characteristics, such as high carbon content, developed pore structures, and improved surface properties, making them suitable for applications including soil amendment, water purification, and electrochemical energy storage. Activated hydrochar derived from waste biomass has shown strong potential as an efficient adsorbent for removing a broad spectrum of pollutants. These contaminants include nutrients such as phosphate from agricultural runoff, as well as synthetic dyes, heavy metals, and pharmaceutical compounds commonly detected in wastewater streams [4-6]. Nevertheless, hydrochar obtained directly from HTC generally requires further chemical or thermal activation to improve its surface area, porosity, and surface functional groups before it can perform effectively as an adsorbent.

In the hydrothermal carbonization (HTC) process, the biomass feedstock is heated to a set temperature and held under controlled conditions for a defined residence time. During the reaction, gaseous products mainly carbon dioxide (CO_2) are generated, along with a liquid phase consisting largely of water containing dissolved organic compounds and fine suspended solids. After completion of the process, the resulting slurry is filtered to separate the liquid phase from the solid material. The recovered solid, often referred to as a wet cake, is then dried to produce hydrochar, a carbon-rich solid product.

Hydrothermal carbonization proceeds through a network of interconnected chemical reactions, including hydrolysis, where biomass interacts with water molecules; dehydration, involving the removal of bound water; decarboxylation, which releases carbon dioxide through the elimination of carboxyl groups; and aromatization, leading to the formation of more stable aromatic structures. These reactions take place under elevated temperature and pressure, resulting in a gradual decrease in the hydrogen-to-carbon (H/C) and oxygen-to-carbon (O/C) ratios and, consequently, an increase in the carbon content of the produced material. As the main solid product of the HTC process, hydrochar possesses versatile characteristics that support its use in a range of applications, including as a solid fuel, an adsorbent for the removal of contaminants such as phosphorus from agricultural runoff, and a soil amendment to enhance soil fertility and structural stability.

The relative amounts of solid, liquid, and gaseous products formed during hydrothermal carbonization are strongly governed by both the characteristics of the biomass feedstock and the applied operating conditions, particularly reaction temperature and residence time. Hydrochar yield, commonly defined as the mass of hydrochar obtained relative to the dry mass of the original feedstock, depends on several factors, including feedstock composition, solids loading (biomass-to-water ratio), reaction temperature, and residence time. In general, increasing process severity through higher temperatures and extended reaction times leads to a reduction in hydrochar yield as a result of intensified degradation of cellulose and hemicellulose fractions. Nevertheless, hydrochar produced under these more severe conditions often displays enhanced carbon enrichment and higher specific surface area, even though the overall mass yield decreases [7].

Agricultural biomass waste mainly comprises residual biological materials originating from plant and animal sources that are generated during the production, harvesting, and processing of agricultural commodities such as fruits, vegetables, grains, crops, dairy products, meat, and poultry. Broadly, agricultural waste can be categorized into four major groups: crop residues (e.g., rice husks, wheat straw, and sugarcane bagasse), animal-derived waste (including manure and carcasses), agro-processing waste (such as packaging materials and fertilizer containers), and hazardous residues, including pesticides and insecticides [5,8,9]. On a global scale, agricultural activities are estimated to produce approximately 998 million tons of waste each year, with nearly 80% of farm-generated solid waste being organic. In many farming systems, this waste is commonly disposed of in pits to free up cultivable land, while some portions are reused as animal feed. However, instead of being treated as a disposal burden, agricultural biomass waste can be transformed into valuable resources. For example, animal manure contains substantial levels of essential nutrients approximately 19% nitrogen, 38% phosphorus, and 61% potassium making it an effective organic fertilizer that can significantly improve soil fertility and agricultural productivity [10,11].

In Nigeria and across many parts of Africa, biomass resources are widely available yet remain largely underexploited, with significant quantities of agricultural residues being discarded as waste, thereby posing environmental concerns. One such residue is the African fan palm nut (*Borassus aethiopum*), which is often thrown away after the edible portion of the fruit is consumed, contributing indirectly to greenhouse gas emissions. Due to its lignocellulosic nature, this biomass represents a promising feedstock for hydrothermal carbonization (HTC), offering a pathway for waste valorization and climate change mitigation. Converting African fan palm nut waste into hydrochar via HTC delivers dual benefits: it reduces the volume of agricultural waste while stabilizing carbon in a solid form, thus supporting long-term carbon sequestration. This strategy aligns with several Sustainable Development Goals, including clean energy, responsible consumption and production, and climate action (United Nations, 2020) [12]. Despite these advantages, studies on the HTC of African fan palm nut particularly regarding its role in carbon capture remain limited, revealing a clear research gap. Effective monitoring and management of this waste stream are therefore essential within the framework of biomass valorization [13]. African fan palm nut waste possesses strong potential as a bioresource, given its relatively high calorific value (approximately 20 kWh/kg), moderate ash content (5-10%), and low moisture content (1–5%). These properties have led to its use as an inexpensive natural biomass fuel [14,15]. Moreover, the widespread availability of African fan palm nut in Nigeria positions it as a renewable, low-cost feedstock for producing efficient and affordable adsorbent materials.

The main aim of this study is to promote the valorization of locally available agricultural waste in Nigeria by reintegrating it into the economic value chain through the production of carbon-based eco-materials using an environmentally friendly and cost-effective hydrothermal process. Specifically, the work examines the suitability of African fan palm nut (AFPN) as a sustainable feedstock for conversion into high-value materials, such as activated carbon. The study also seeks to produce activated carbon that satisfies the quality specifications outlined in the Indonesian National Standard (SNI 06-3730-1995), ensuring compliance with critical performance criteria. To achieve optimal hydrochar production, Response Surface Methodology (RSM) was applied to identify the most favorable operating conditions. Furthermore, Energy Dispersive X-ray Fluorescence (EDXRF) analysis was used to evaluate the elemental composition of the synthesized hydrochar, providing insight into its suitability for applications such as adsorption, catalysis, and soil amendment. The African fan palm (*Borassus aethiopum*) tree, fruit and nut used as biomass feedstock in this study are shown in Fig. 1.



Fig 1: African fan palm tree, fruit and nut used as feedstock for the hydrothermal carbonization process.

2.0 Materials and methods

2.1 Feedstock preparation

The African fan palm nut (AFPN) feedstock for this study was collected in bulk from a farm refuse site at Nnamdi Azikiwe University, Awka, Anambra State, Nigeria. To reduce moisture and prepare the material for processing, the AFPN was thoroughly washed and sun-dried for three days. Once dried, the nuts were manually crushed with a hammer, and the kernels were carefully separated from their shells. The kernels underwent a pretreatment step by soaking in a 4 g dm^{-3} sodium hydroxide solution for 72 hours to remove impurities and pigments, with gentle stirring every 24 hours to prevent coagulation. After pretreatment, the AFPN was rinsed three times with running tap water and sun-dried for an additional three days. The material was further dried in a laboratory oven at 101 °C until the moisture content dropped below 10 wt.%. The dried kernels were then pulverized using an industrial ball mill at Eke-Awka Market, Awka, Nigeria, and the resulting powder was sieved through a 300 µm mesh to ensure uniform particle size suitable for hydrochar production. Finally, 50 g of the sieved powder was accurately weighed with an electronic balance to prepare it for the hydrothermal carbonization (HTC) experiments.

2.2 Hydrochar Production

The hydrochar production process was optimized using Response Surface Methodology (RSM) in combination with a Central Composite Design (CCD). The experimental design was carried out using Design-Expert software (version 10) and focused on three key independent variables: reaction temperature, reaction time, and the biomass-to-water ratio. A total of fifteen experimental runs were performed, as summarized in Table 1, with hydrochar yield serving as the primary response variable.

2.2.2 Analysis of the responses

The hydrochar yield for each sample was measured using a digital analytical balance. The results were recorded meticulously and expressed as a percentage of the initial dry biomass. Calculations were

performed based on standard equations derived from the hydrothermal carbonization (HTC) process, as outlined below:

$$\%\, Yield_{HC} = \frac{\text{weight of hydrochar}}{\text{weight of Biomass}} \times 100 \quad (1)$$

$$\%\, Yield_{BO} = \frac{\text{weight of Bio-oil}}{\text{weight of Biomass}} \times 100 \quad (2)$$

While the gaseous products and the water account for the percentage mass difference were calculated by:

$$\%\, Yield_{gas} = 100\% - \%\, Yield_{BO} - \%\, Yield_{HC} \quad (3)$$

Where $\%\, Yield_{BO}$, $\%\, Yield_{HC}$, $\%\, Yield_{gas}$ are the percentage weight yield for hydrochar, bio-oil, and a mixture of gas and water, respectively.

2.2.3 Hydrothermal carbonization

Hydrothermal carbonization (HTC) of African fan palm nut (AFPN) was carried out in a sealed autoclave reactor to investigate how the final reaction temperature and residence time affect the physicochemical properties of the resulting hydrochar and bio-oil. In each experiment, the reactor was gradually heated to the target temperature, which was then maintained for the specified reaction time to ensure thorough and effective carbonization.

Table 1 HTC Factors for Hydrochar Production

Factor	Name	Unit	Low level	High level
A	Reaction Temperature	℃	180.00	220.00
B	W-B Ratio	g	8.00	12.00
C	Reaction Time	min	30.00	90.00
D	Heating Rate	℃/min	5.00	6.00

A Type-K thermocouple (RS Pro) equipped with a data logger was installed at the upper section of the reactor to continuously monitor the internal temperature throughout the hydrothermal carbonization process. The experiments were conducted in three separate series. In the first series, reaction temperatures of 180, 200, and 220 °C were applied with a fixed residence time of 30 minutes, producing hydrochar samples labeled AFPNH200 (30 min) and AFPNH220 (30 min). In the second series, the same temperature range was used while the residence time was extended to 60 minutes, resulting in samples coded AFPNH200 (60 min) and AFPNH220 (60 min). The third series maintained the same temperatures with a 90-minute residence time, yielding hydrochar samples AFPNH200 (90 min) and AFPNH220 (90 min).

After each run, the reactor was allowed to cool naturally to room temperature. The resulting slurry was filtered using Whatman Grade 1 filter paper (11 µm) with a Büchner funnel to separate the solid hydrochar from the liquid phase. The recovered hydrochar was thoroughly washed with deionized water to remove residual process liquids and then air-dried at room temperature for three days to reduce moisture content. Finally, the dried hydrochar was weighed to determine the mass yield. The hydrothermal carbonization procedure was repeated for all biomass samples across the different temperature and residence-time conditions. The solid fraction was separated from the bio-oil using filter paper and sun-dried to remove any remaining moisture. The masses of the dried hydrochar and the residual bio-oil were then measured using an LWS-3C digital analytical balance, and all experimental observations were carefully documented.

2.2.4 Hydrochar Yield Optimization

The main process variables influencing hydrochar production, reaction temperature, water-to-biomass ratio, and residence time were optimized using Design-Expert software based on the experimental response data. The software's optimization module was employed to determine the best combination of factor levels that met predefined criteria for both process parameters and response outcomes. Numerical optimization techniques guided this analysis, with target goals for each factor and response defined through the criteria settings. This allowed responses to be maximized, minimized, targeted, or constrained within specific ranges, while input factors were assigned fixed or bounded values. To achieve improved hydrochar quality and yield, the optimization was designed to maximize hydrochar yield, specific surface area, and pore volume, while minimizing bio-oil production.

2.3 Characterization of Hydrochar

This section outlines the analytical techniques employed to characterize the hydrochar produced in this study, detailing the methods used to evaluate its physicochemical and structural properties.

2.3.1 Ultimate (Elemental) Analysis

Total nitrogen (N) content was determined using the Kjeldahl method, while the concentrations of carbon (C), hydrogen (H), sulfur (S) and oxygen (O), were measured with a CHNSO analyzer (LECO CHNSO 628 Series) in accordance with ASTM D5373. Oxygen (O) content was estimated by difference, calculated as 100% minus the combined weight percentages of carbon, hydrogen, nitrogen, sulfur, and ash. The molar ratios of O/C and H/C were subsequently computed from the measured elemental compositions.

2.4 Determination of Moisture Content

The powdered samples were dried in a sealed Memmert oven at 105 °C for 10 minutes to remove moisture. Each sample was placed in a pre-weighed stainless-steel pan. After drying, the pans with the samples were allowed to cool to room temperature and then reweighed. This drying and weighing cycle was repeated until a constant weight was obtained. Multiple replicates were conducted for each sample to ensure accuracy, and the reported values represent the average weight.

$$\text{Moisture content}(\%) = \frac{W_i - W_f}{W_i} \times 100 \quad (4)$$

Where, W_i = initial weight of the sample, W_f = final weight of the sample after drying.

2.5 Determination of Volatile Matter

The volatile matter content of the samples was measured using the Meynell method. Dry samples obtained from the moisture analysis were initially preheated at 280 °C for 2 hours to drive off volatile components. They were then further heated at 450 °C for an additional 2 hours until complete conversion to ash. The weights of the samples were recorded before and after heating to calculate the volatile matter content.

The volatile matter content was calculated using the following expression:

Volatile Matter (%) =Weight of residual dry sample -Weight of dry sample after heating

$$\% \text{ Volatile Matter} = \frac{W_{rd} - W_{ds}}{W_{st}} \times 100 \quad (5)$$

Where W_{rd} = weight due to removal of the volatile matter, W_{ds}= weight of dry sample after heating, W_{st} = weight of sample taken

2.5.1 Ash content of the samples

One gram of each previously dried sample was placed in a furnace and heated at 630 °C for about 1 hour. After heating, the samples were allowed to cool to room temperature in a desiccator before being weighed. This procedure was repeated for all samples, and the average of the measurements was reported as the final ash weight.

$$\text{Ash content}(\%) = \frac{W_a}{W_i} \times 100 \quad (6)$$

Where, W_a = weight of the ash, W_i= initial weight of dried sample.

2.5.2 Fixed carbon content of the samples

The fixed carbon content of the samples was calculated using the equation below. Fixed carbon represents the solid carbon residue remaining in the biomass after devolatilization [15]:

$$\text{Carbon content } (\%) = 100\% - (\%AC - \%VM - \%MC) \quad (7)$$

Where, AC = Ash content, VM = Volatile Matter, MC = Moisture Content.

2.5.2.1 H/C and O/C Ratio

The carbon (C), hydrogen (H), and oxygen (O) contents measured through CHNSO analysis were used to calculate the hydrogen-to-carbon (H/C) and oxygen-to-carbon (O/C) atomic ratios for the African Fan Palm Nut, hydrochar, and activated hydrochar samples. These atomic ratios were determined using Equations (8) and (9) as outlined by [16].

$$H/C = \frac{Percentage\ Weight\ of\ Hydrogen / Molar\ weight\ of\ Hydrogen}{Percentage\ weight\ of\ Carbon / Molar\ Weight\ of\ Carbon} \quad (8)$$

$$O/C = \frac{Percentage\ Weight\ of\ Oxygen / Molar\ weight\ of\ Oxygen}{Percentage\ weight\ of\ Carbon / Molar\ Weight\ of\ Carbon} \quad (9)$$

The density of each sun-dried biochar sample was determined using a relative density bottle. The masses of the empty bottle (m_1), bottle with biochar (m_2), bottle with biochar and water (m_3), and bottle with water only (m_4) were measured using a digital balance. The mass of water corresponding to the bottle volume was calculated as ($m_4 - m_1$), while the mass of water displaced by the biochar was obtained from $m_4 - m_1) - (m_3 - m_2)$. These values were then used to calculate the relative density (R_{hc}) and the actual density (ρ_b) of the biochar using the standard equations (10) and (11) (Odeh et al., 2025) (17).

$$R_{hc} = \frac{mass of hydrochar}{mass of equal volume of water} = \frac{(m_2 - m_1)}{(m_4 - m_1) - (m_3 - m_2)} \quad (10)$$

$$\rho_{hc} = R_{hc} \times density of water \quad (11)$$

3 Results and discussion

3.1 Experimental Findings

Table 2 summarizes the results of the experimental design and the corresponding hydrochar production responses. The highest hydrochar yield, 48.61 g, was achieved at a reaction temperature of 180 °C, a residence time of 30 minutes, a heating rate of 4 °C/min, and a water-to-biomass ratio of 12 g. In contrast, the lowest hydrochar yield of 23.44 g was observed at 220 °C, 90 minutes, a heating rate of 4 °C/min, and the same water-to-biomass ratio. The maximum bio-oil yield of 30.72 g occurred at 220 °C, 90 minutes, a heating rate of 7 °C/min, and a water-to-biomass ratio of 12 g.

Table 3 presents the model fit for the hydrochar yield response. The optimal model was chosen based on a p-value below 0.05, indicating statistical significance, and the absence of aliasing, which ensures clear and unambiguous interpretation. Additionally, the close agreement between the adjusted R^2 and predicted R^2 values confirms the model's reliability for predictive purposes. Based on these assessments, the linear model with a p-value less than 0.0001 is recommended. This high level of significance demonstrates that the model effectively captures the relationship between the independent variables and hydrochar yield, making it a robust tool for further analysis and interpretation.

The sequential model sum of squares for the hydrochar yield response, shown in Table 4, was used to identify the highest-order polynomial model that included statistically significant terms without any evidence of aliasing. Based on this assessment, the Linear vs. Mean model was selected for further analysis. This model had a sum of squares of 1489.12 with 4 degrees of freedom (df). The choice was based on its statistical significance and its ability to adequately explain the variability in the response. As a result, the selected model reliably captures the key relationships within the experimental data and provides a robust foundation for subsequent analysis.

Table 2 The experimental design, and the responses obtained from the produced hydrochar

Runs	Temperature (° C)	Residence Time (mins)	Heating Rate (° C/mins)	Biomass to Water (g)	Char Yield (%)	Oil Yield (%)
1	180	30	4	8	47.50	19.35
2	220	30	4	8	28.80	28.40
3	180	30	4	12	48.61	20.81
4	220	30	4	12	29.62	28.31
5	180	90	4	8	46.81	21.24
6	220	90	4	8	25.21	28.70
7	180	90	4	12	44.65	23.04
8	220	90	4	12	23.44	29.16
9	180	30	7	8	46.51	20.82
10	220	30	7	8	27.10	30.20
11	180	30	7	12	46.15	21.81
12	220	30	7	12	26.80	29.20
13	180	90	7	8	43.02	25.91
14	220	90	7	8	29.91	29.10
15	180	90	7	12	45.61	26.34
16	220	90	7	12	24.80	30.72
17	200	60	5.5	10	38.11	29.31

Table 3 Fit summary for char yield response

Source	Sequential p-value	Lack of Fit p-value	Adjusted R^2	Predicted R^2	
Linear	< 0.0001		0.9652	0.9467	Suggested
2FI	0.5426		0.9636	0.8762	
Quadratic	0.4631		0.9612		Aliased

Table 4 Sequential model sum of squares for char yield response

Source	Sum of Squares	df	Mean Square	F-value	p-value	
Mean vs Total	22806.42	1	22806.42			
Linear vs Mean	1489.12	4	372.28	111.85	< 0.0001	Suggested
2FI vs Linear	19.06	6	3.18	0.9130	0.5426	
Quadratic vs 2FI	2.34	1	2.34	0.6309	0.4631	Aliased
Residual	18.54	5	3.71			
Total	24335.48	17	1431.50			

Table 5 ANOVA for linear model (char yield response)

Source	Sum of Squares	df	Mean Square	F-value	p-value

Model	1489.12	4	372.28	111.85	< 0.0001	significant
A-Reaction Temperature	1466.58	1	1466.58	440.64	< 0.0001	
B-W-B Ratio	1.68	1	1.68	0.5050	0.4909	
C-Reaction Time	19.46	1	19.46	5.85	0.0324	
D-Heating Rate	1.40	1	1.40	0.4205	0.5289	
Residual	39.94	12	3.33			
Cor Total	1529.06	16				

3.1.1 ANOVA results for the linear model of char yield response

Table 5 presents the Analysis of Variance (ANOVA) results for the linear model used to assess hydrochar yield. The model exhibits a high F-value of 111.85, indicating strong statistical significance and suggesting that the likelihood of this result occurring due to random chance is only about 0.01%. All model terms included have P-values below 0.0500, confirming their statistical relevance, with factors A and C highlighted as particularly significant contributors. Terms with P-values exceeding 0.1000 are considered statistically insignificant. These results confirm the adequacy and reliability of the selected model in capturing the variability observed in hydrochar yield.

Equation (13) defines the mathematical model for char yield expressed using the actual process variables.

$$\text{Char Yield} = 137.27778 - 0.478700A - 0.162062B - 0.036758C - 0.197167D \quad (12)$$

The model, expressed in terms of actual factors, allows for the prediction of hydrochar yield at specific levels of each variable. This predictive capability was used to generate a plot comparing the model's predicted values with the experimental results, as illustrated in Fig. 2.

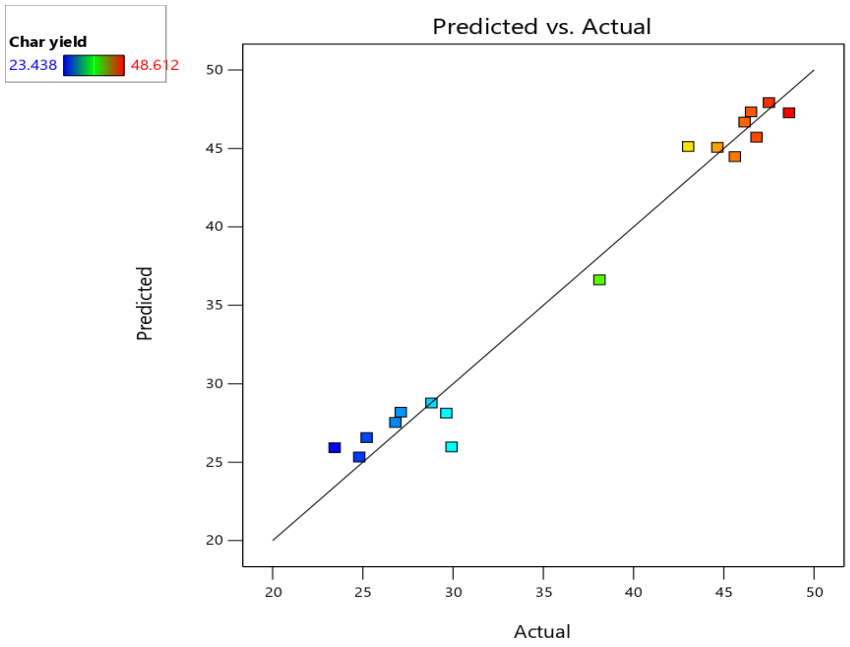


Figure. 2 Graph of Predicted versus actual plot for char yield

Figure 2 shows the comparison between the predicted and experimentally measured hydrochar yield values. The plot reveals a strong correlation between the model predictions and the observed data, with experimental points clustering closely around the line representing the predicted response. This close alignment indicates high model reliability and predictive accuracy. The normal distribution of the data further confirms that the selected model adequately represents the hydrochar yield response. Therefore, the Central Composite Design (CCD) demonstrates a good fit and can be confidently used for optimization studies.

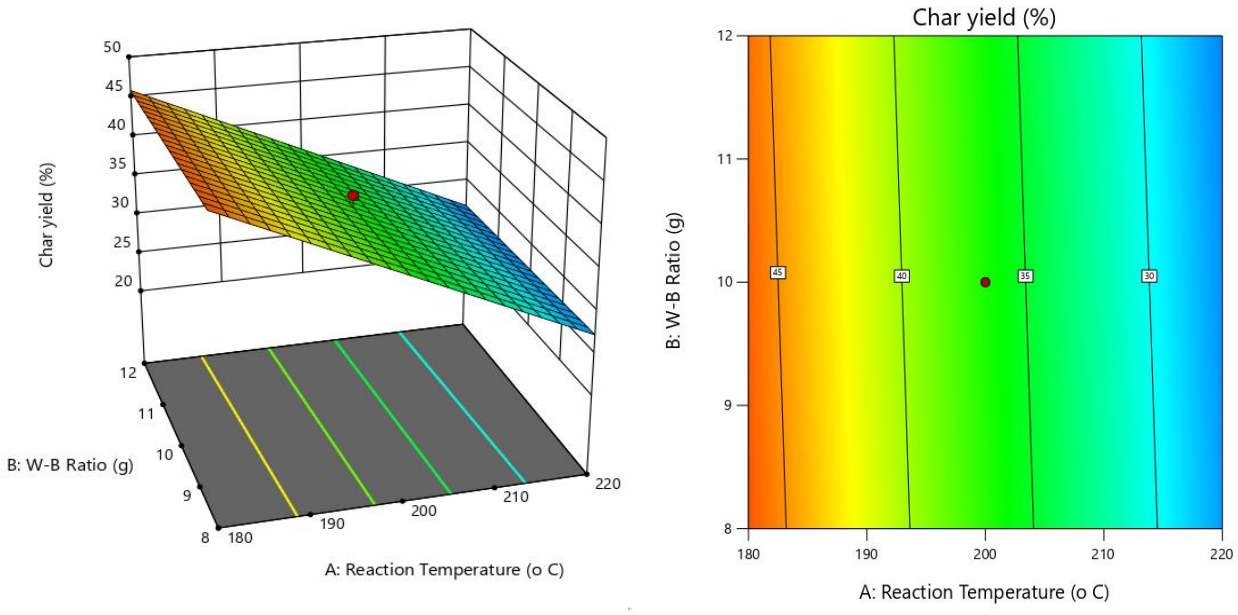


Fig. 3 3D response surface plot and contour of temperature and water-biomass ratio on percentage char yield

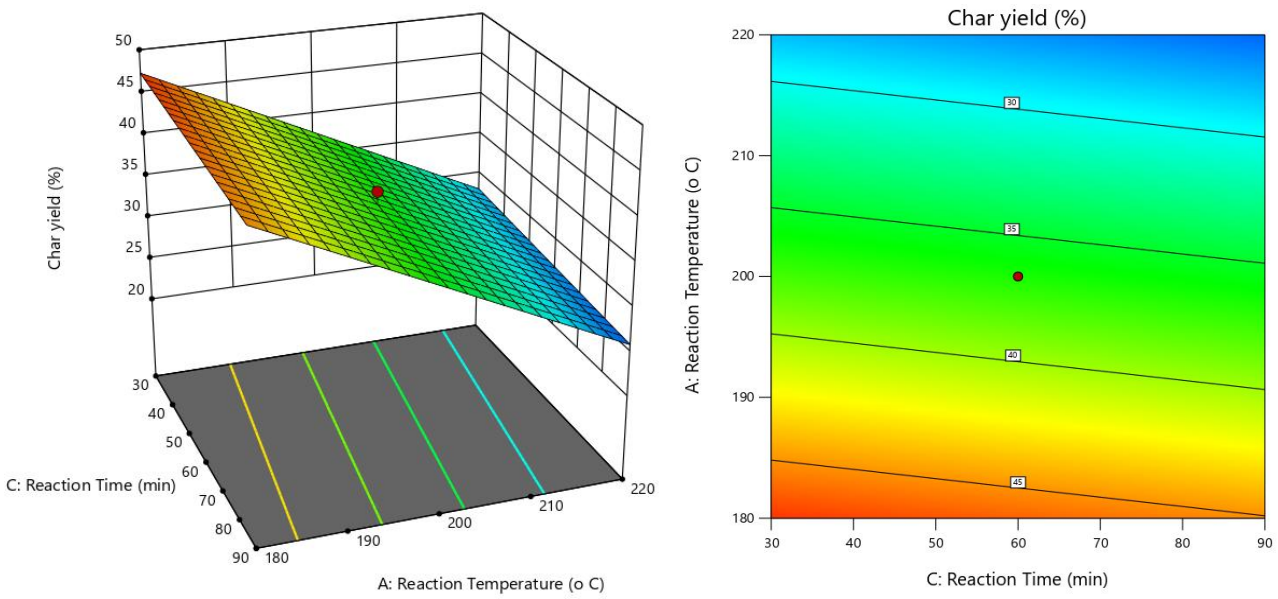


Fig. 4 3D response surface plot and contour of temperature and residence time on percentage char yield

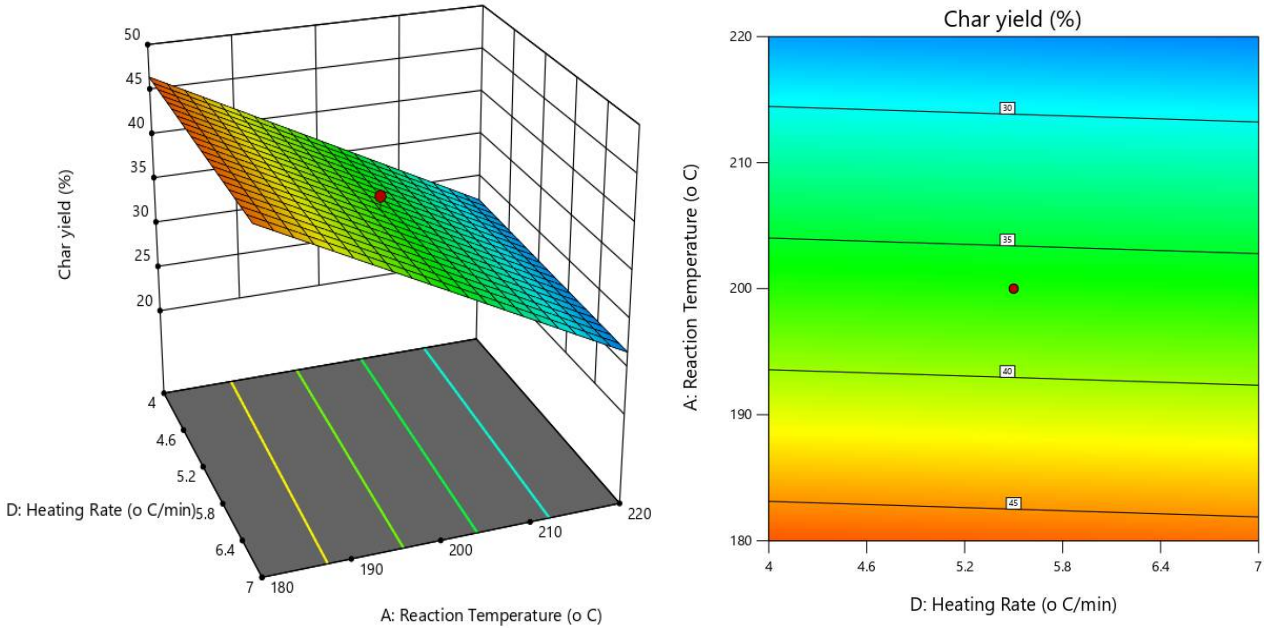


Fig. 5 3D response surface plot and contour of temperature and heating rate on percentage char yield

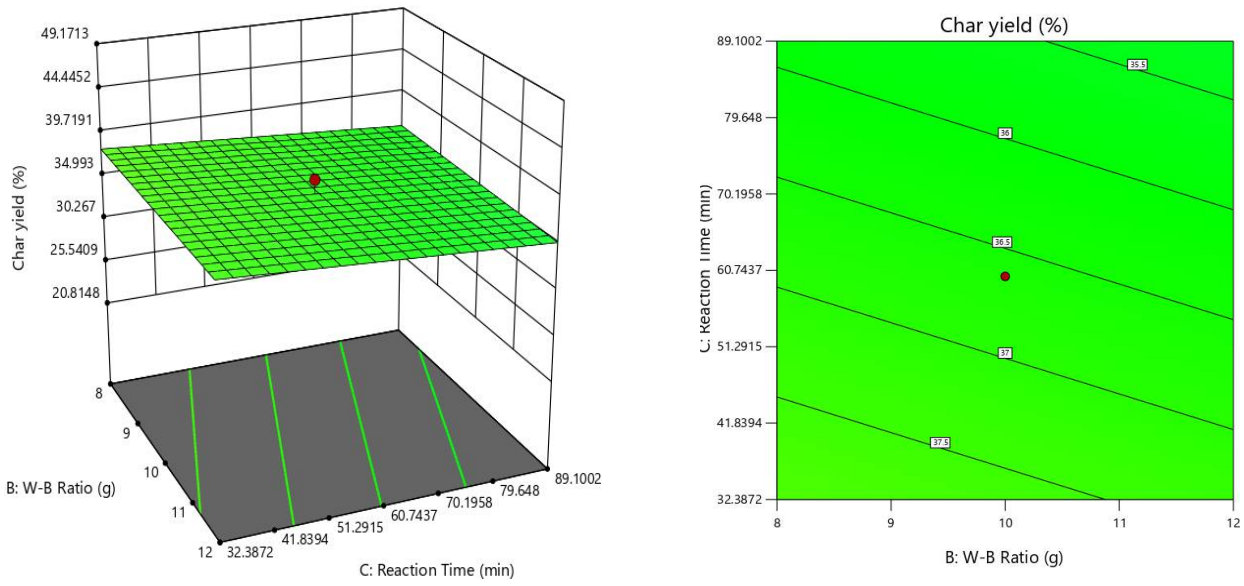


Fig. 6 3D response surface plot and contour of W-B ratio and residence time on percentage char yield

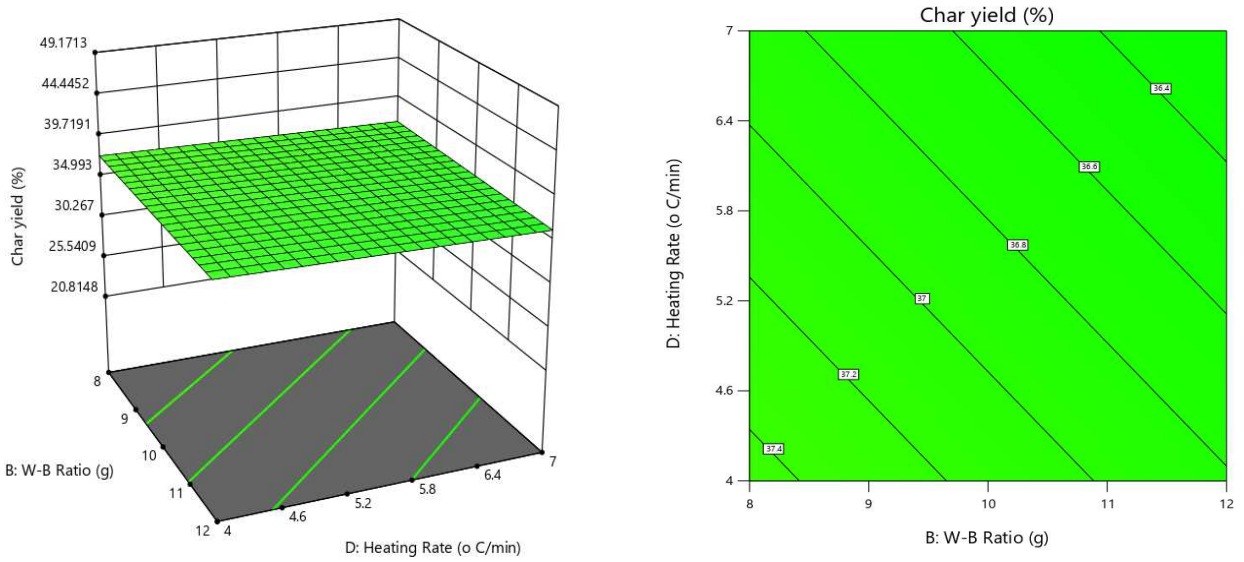


Fig. 7 3D response surface plot and contour of W-B ratio and heating rate on percentage char yield

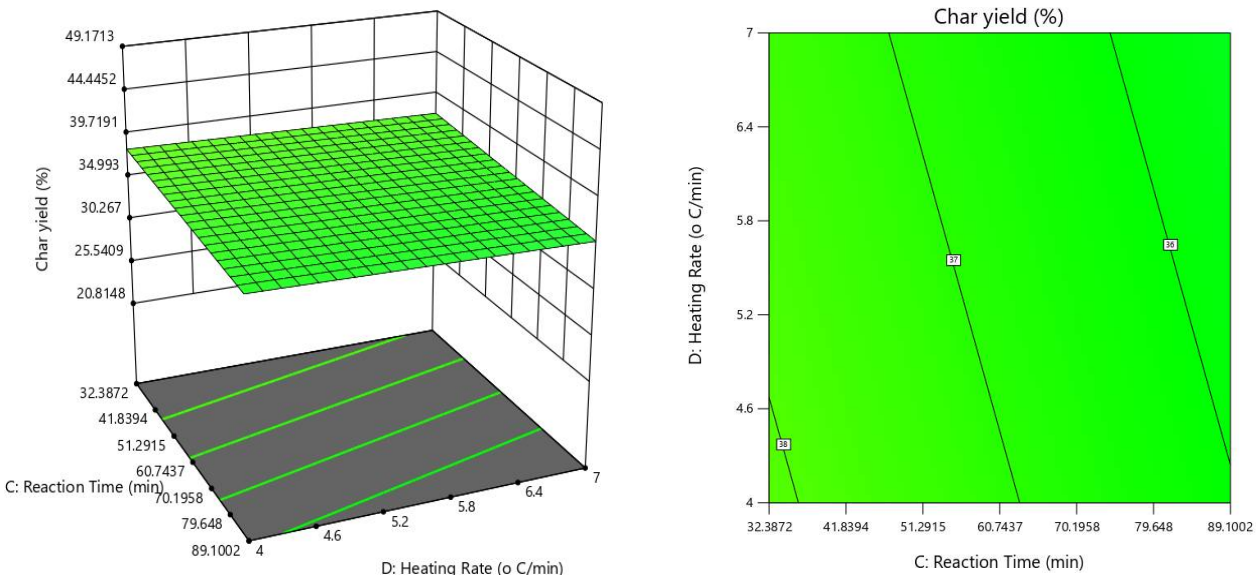


Fig. 8 3D response surface plot and contour of residence time and heating rate on percentage char yield

3.2 Combined Influence of Process Parameters on Char Yield

As illustrated in Figure 3, hydrochar yield is relatively high at low to moderate reaction temperatures but decreases as the temperature increases further. This trend can be attributed to incomplete conversion and oil extraction from the biomass at lower temperatures, which results in a higher solid residue [17]. At higher temperatures, however, more of the solid char is converted into liquid and gaseous products, increasing bio-oil and gas formation and reducing hydrochar yield. The contour plot reinforces this behavior, showing a minimum char yield of approximately 30 % at 214 °C with a water-to-biomass ratio of 10 g, while the maximum yield of around 45 % occurs at a lower temperature of 183 °C combined with a slightly higher water-to-biomass ratio of 10.2 g. The color gradients in Figure 3 further confirm that lower temperatures and higher water-to-biomass ratios favor char formation, whereas higher temperatures and lower ratios lead to reduced yields. These observations underscore the importance of carefully optimizing both temperature and water-to-biomass ratio to maximize hydrochar production in the HTC

Figure 4 presents the three-dimensional response surface and contour plots illustrating the combined effects of temperature (T) and residence time (Rt) on hydrochar yield during hydrothermal carbonization (HTC). The results show that both factors significantly influence char formation, with temperature having a more pronounced effect than residence time. As shown in Figure 4, higher hydrochar yields are achieved at relatively lower temperatures and shorter residence times. This trend is primarily due to the increased generation and release of gaseous products at higher temperatures, which reduces the solid char output a behavior consistent with previous studies [18,19].

Figure 5 presents the three-dimensional response surface and contour plots showing the interactive effects of temperature (T) and heating rate (Hr) on hydrochar yield during hydrothermal carbonization (HTC). The results indicate that both factors significantly influence char production, with temperature exerting a stronger effect than the heating rate. As illustrated in Figure 5, the highest hydrochar yields are obtained at relatively lower temperatures combined with moderate heating rates. This pattern is

mainly due to the increased formation and release of gaseous by-products at higher temperatures, which reduces the solid char fraction a trend that has been reported in previous studies.

Figure 6 shows the three-dimensional response surface and contour plots depicting the combined effects of the water-to-biomass ratio (W-B) and residence time (Rt) on hydrochar yield, with all other variables held at their central levels. The plots indicate that both factors significantly influence char production, highlighting the need to carefully optimize these process parameters to maximize hydrochar yield.

Figure 7 presents the three-dimensional response surface and contour plots illustrating the combined effects of the biomass-to-water ratio (W-B) and heating rate (Hr) on hydrochar yield during hydrothermal carbonization (HTC). Within the studied range, both factors have a relatively minor impact on char production. Nevertheless, a slight decrease in hydrochar yield is observed as both the biomass–water ratio and heating rate increase, indicating a subtle but discernible negative trend.

Figure 8 illustrates the three-dimensional response surface and contour plots showing the combined effects of residence time (Rt) and heating rate on hydrochar yield during hydrothermal carbonization. The relatively flat response surfaces indicate that variations in these parameters have only a minimal impact on char yield within the studied range. This suggests that neither residence time nor heating rate, individually or in combination, significantly influences the formation of solid char.

3.3 Analysis of bio-oil yield

3.3.1 Fit summary for bio-oil yield response

Table 6 presents the model fit for the bio-oil yield response. The selected model is considered appropriate, with a p-value below 0.05, indicating it is free from aliasing and shows strong agreement between the adjusted R^2 and predicted R^2 values. Based on these criteria, the linear model, with a p-value of less than 0.0001, was chosen for further analysis. This high level of statistical significance confirms that the model effectively captures the key factors influencing bio-oil yield.

3.3.2 Sequential model sum of squares for bio-oil yield response

The sequential model sum of squares for the bio-oil yield response, shown in Table 7, was used to identify the highest-order polynomial model that includes statistically significant terms without aliasing. Based on this evaluation, the Linear versus Mean model was selected, with a sum of squares of 214.74 and 4 degrees of freedom (df). This model was chosen because it effectively explains the observed variability in bio-oil yield while including only statistically meaningful terms.

3.3.3 ANOVA results for the linear model of char yield response

Table 8 summarizes the ANOVA results for the linear model evaluating hydrochar yield. The model shows an F-value of 20.53, indicating strong statistical significance, with only a 0.01% chance of this value arising from random variation. All model terms have P-values below 0.0500, confirming their significance, with factors A, C, and D identified as key contributors. Conversely, terms with P-values above 0.1000 are considered statistically insignificant, highlighting the importance of the selected terms in explaining the observed variability in hydrochar yield.

Equation (14) expresses the bio-oil yield model as a function of the actual process variables.

Oil Yield = -14.24501 + 0.170194A + 0.086125B +0.031908C + 0.628500D (13)

The model equation expressed in actual factor units can be used to predict the response at specific levels of each variable. However, this form is not ideal for evaluating the relative impact of individual factors, since the coefficients are influenced by the units of the variables and the intercept is not centered within the design space. Therefore, the model in Equation (13) was used to generate the predicted-versus-actual response plot presented in Figure 9.

Figure 9 shows the comparison between the predicted and experimentally measured bio-oil yield values. The plot demonstrates strong agreement, with experimental points closely clustered around the line of predicted values from Equation (13). This alignment indicates a normal distribution of residuals and confirms that the model accurately predicts bio-oil yield. These results further demonstrate that the Central Composite Design (CCD) provides a robust fit and can be confidently used for process optimization.

Table 6 Fit summary for oil yield response

Source	Sequential p-value	Lack of Fit p-value	Adjusted R^2	Predicted R^2	
Linear	< 0.0001		0.8300	0.7754	Suggested
2FI	0.5371		0.8233	0.7263	
Quadratic	0.0184		0.9371		Aliased

Table 7 Sequential model sum of squares for oil yield response

Source	Sum of Squares	df	Mean Square	F-value	p-value	
Mean vs Total	11515.20	1	11515.20			
Linear vs Mean	214.74	4	53.68	20.53	< 0.0001	Suggested
2FI vs Linear	15.07	6	2.51	0.9237	0.5371	
Quadratic vs 2FI	11.47	1	11.47	11.85	0.0184	Aliased
Residual	4.84	5	0.9682			
Total	11761.32	17	691.84			

Table 8 ANOVA for linear model (char yield response)

Source	Sum of Squares	df	Mean Square	F-value	p-value	
Model	214.74	4	53.68	20.53	< 0.0001	significant
A-Reaction Temperature	185.38	1	185.38	70.89	< 0.0001	
B-W-B Ratio	0.4747	1	0.4747	0.1815	0.6776	
C-Reaction Time	14.66	1	14.66	5.61	0.0355	
D-Heating Rate	14.22	1	14.22	5.44	0.0379	

Residual	31.38 12	2.61
Cor Total	246.12 16	

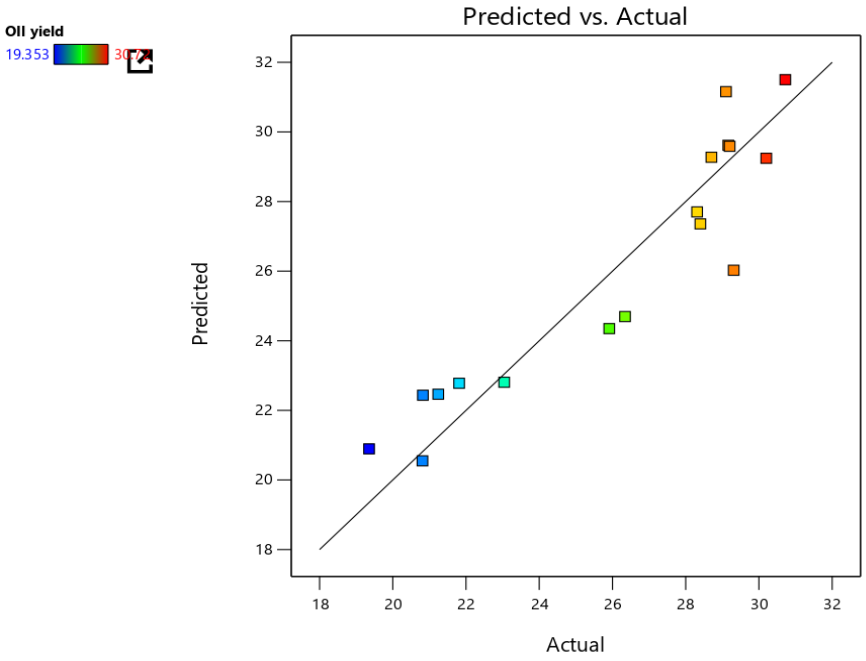


Fig. 9 Graph of predicted versus actual plot for bio-oil yield

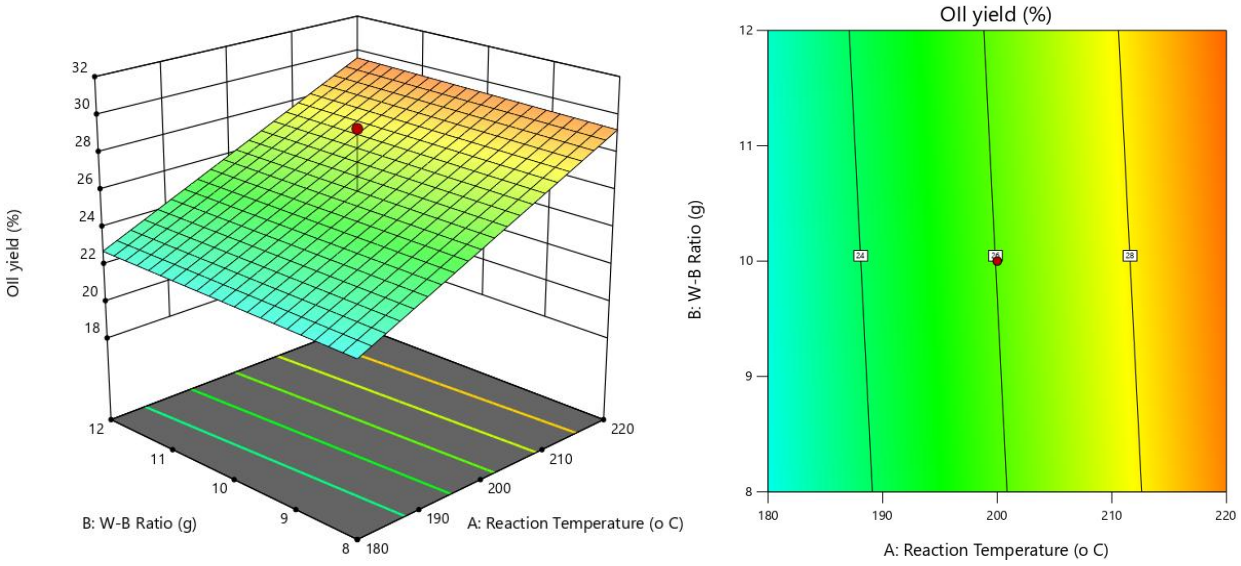


Figure 10 3D response surface plot and contour of temperature and water-biomass ratio on percentage Oil yield

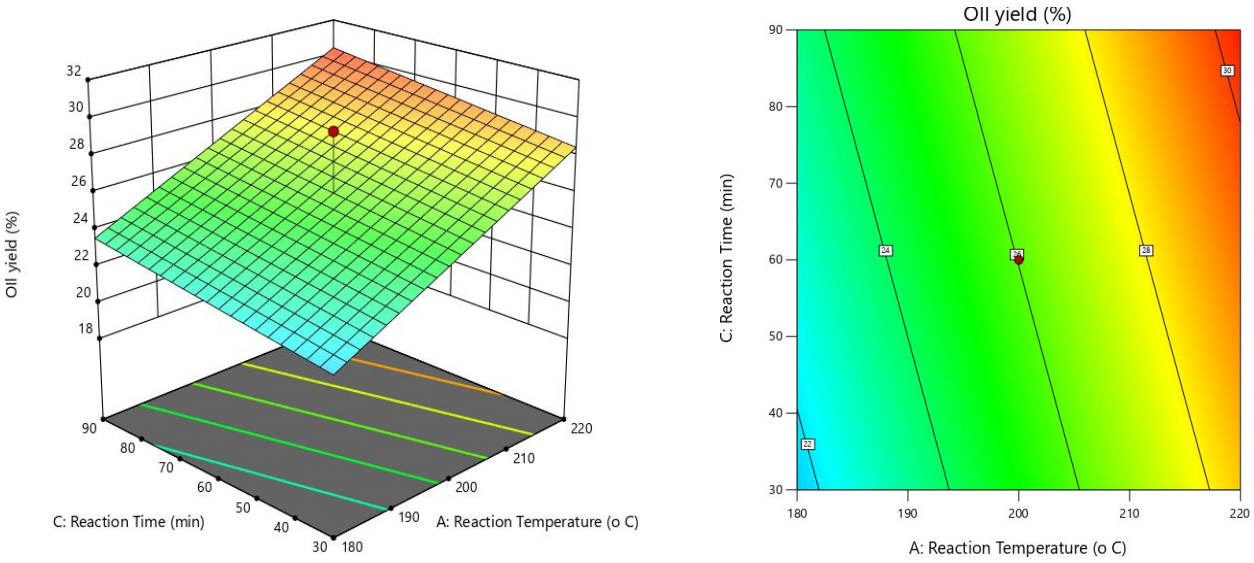


Figure 11 3D response surface plot and contour of temperature and residence time on percentage Oil yield

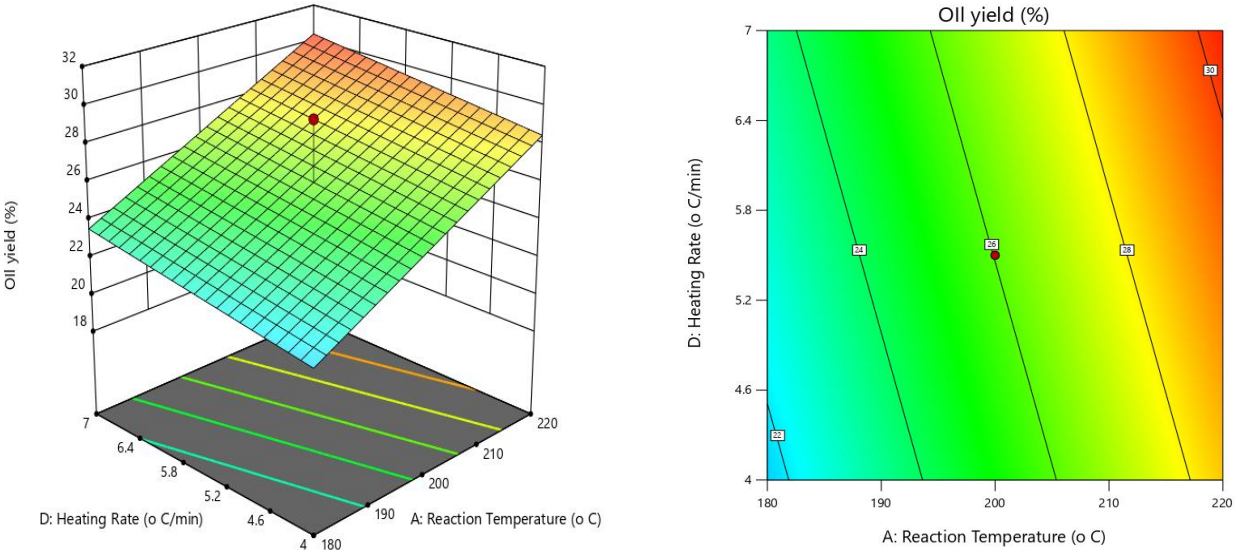


Figure 12 3D response surface plot and contour of temperature and heating rate on percentage Oil yield

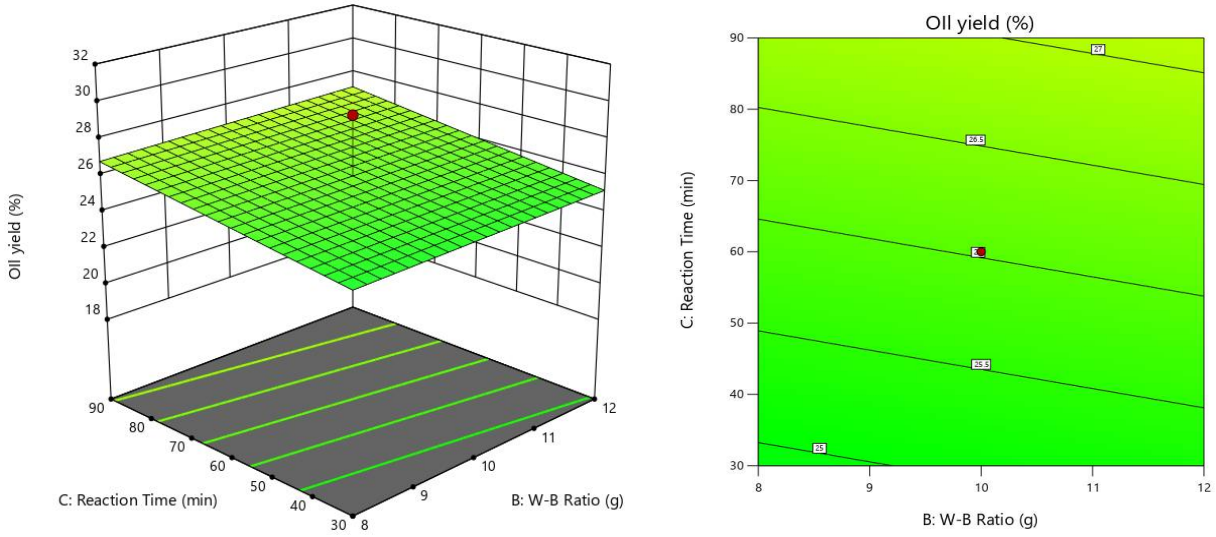


Figure 13 3D response surface plot and contour of W-B ratio and residence time on percentage Oil yield

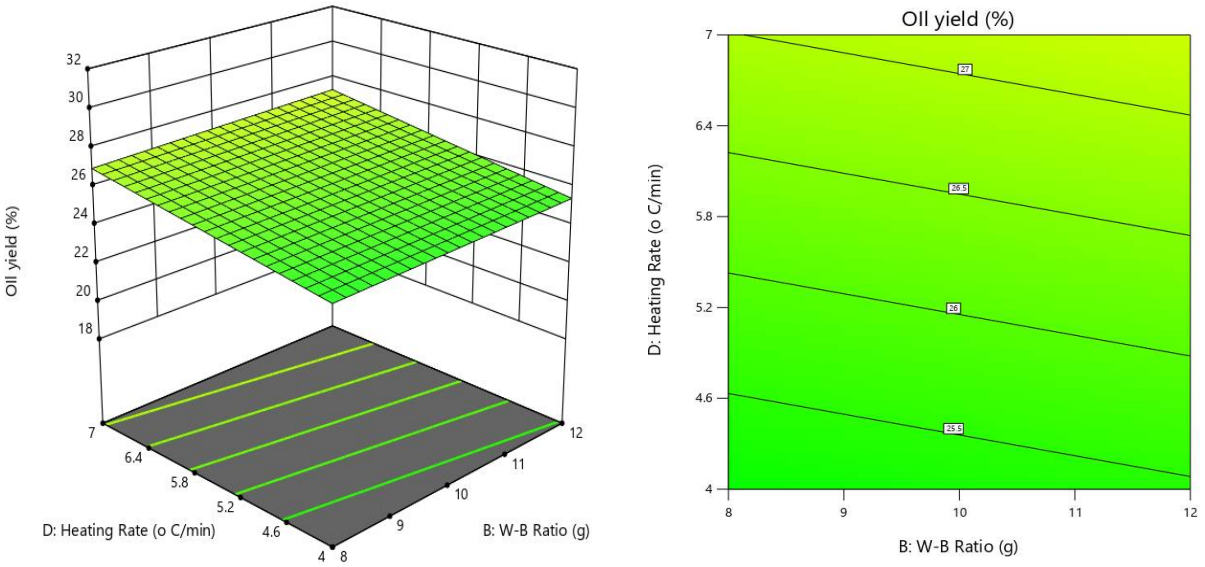


Figure 14 3D response surface plot and contour of W-B ratio and heating rate on percentage Oil yield

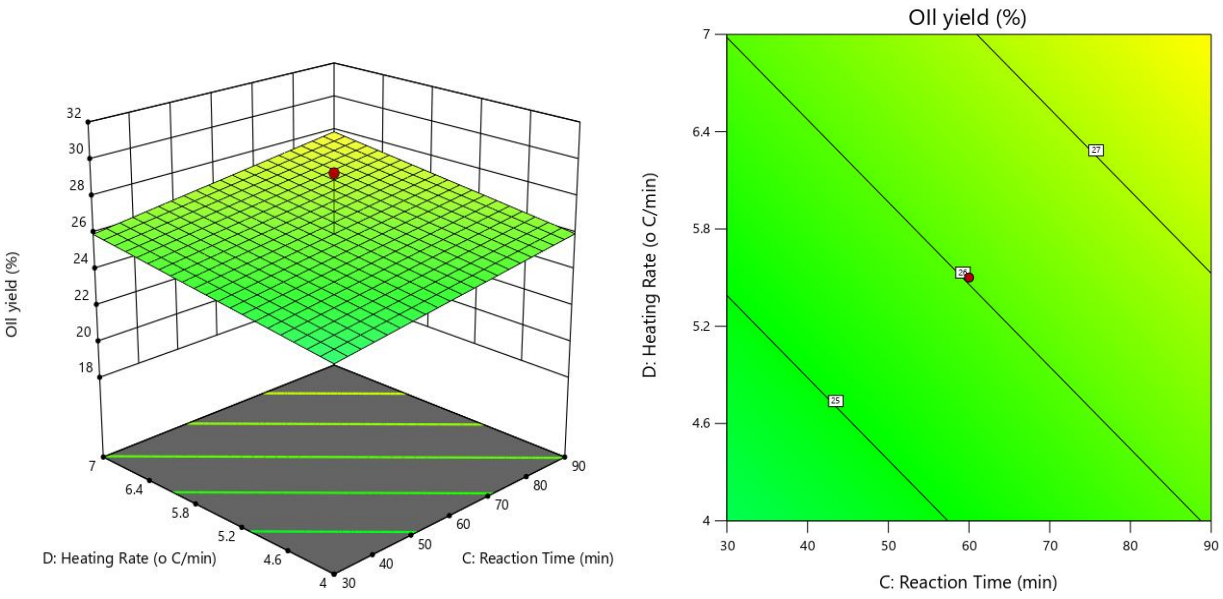


Figure 15 3D response surface plot and contour of residence time and heating rate on percentage Oil yield

3.4 Combined Influence of Process Parameters on Oil Yield

Figure 10 presents the three-dimensional response surface and corresponding contour plots that describe how temperature (T) interacts with the water-biomass (W-B) ratio to influence bio-oil yield. These plots were developed to assess the combined impact of these two variables while all other process conditions were held constant. As shown in Fig. 10, increasing both the reaction temperature and the W-B ratio generally leads to an improvement in bio-oil yield. This trend is linked to more effective conversion of lignocellulosic components when moderate thermal conditions are applied.

At relatively low temperatures (below about 280 °C), biomass depolymerization is insufficient, resulting in lower bio-oil production. In contrast, very high temperatures (above roughly 350 °C) tend to promote the formation of gaseous products and water-soluble compounds rather than bio-oil. The contour plot further emphasizes that both reaction temperature and the W-B ratio play a significant role in determining bio-oil yield. A minimum yield of 24% occurs at a W-B ratio of 10.1 g and a temperature of 188 °C, while the maximum yield of 28% is observed at a W-B ratio of 10.5 g and a temperature of 213 °C. These findings underscore the importance of carefully optimizing both the water-biomass ratio and reaction temperature to achieve higher bio-oil yields during the hydrothermal carbonization process.

Figure 11 illustrates the three-dimensional response surface together with the associated contour plots that describe the combined influence of reaction temperature and residence time on bio-oil yield. In this analysis, both variables were systematically varied while all other independent parameters were maintained at their central values. The 3D surface clearly shows that residence time plays a key role in determining bio-oil yield. Longer residence times during hydrothermal carbonization (HTC) favor increased bio-oil production, as HTC is typically conducted at lower temperatures than pyrolysis and therefore requires extended reaction periods to enable effective oil formation. The contour plot further demonstrates the interactive relationship between temperature and residence time in controlling bio-oil

yield. The highest yield, approximately 30%, is achieved at a temperature of 218 °C and a residence time of 85 min, while the lowest yield, around 22%, is observed at 182 °C and 37 min. Consistent with the observations of Akhtar et al. [20], these results suggest that the negative effect of shorter residence times on oil production can be mitigated by operating at higher temperatures, whereas longer residence times are needed to compensate for lower reaction temperatures.

Figure 12 presents the three-dimensional response surface and the associated contour plots that show how temperature (T) and heating rate (Hr) jointly affect oil yield during hydrothermal carbonization (HTC). The results demonstrate that both variables play important roles in oil formation, although temperature has a more pronounced effect than the heating rate. As illustrated in the figure, maximum oil yields are achieved at higher temperatures, around 219 °C, in combination with a relatively high heating rate of 6.8 °C/min. This trend can be explained by intensified thermal reactions at elevated temperatures, which enhance the generation and release of volatile intermediates that later condense to form the liquid oil phase. Similar patterns have been observed in previous studies, indicating good agreement with earlier reported findings.

Figure 13 shows the three-dimensional response surface together with the corresponding contour plots that describe how residence time interacts with the water-biomass (W-B) ratio to affect bio-oil yield. The results indicate that the highest bio-oil yield, approximately 27%, is achieved at a W-B ratio of 11 g and a residence time of 88 min, while the lowest yield, about 25%, occurs at a W-B ratio of 8.6 g and a residence time of 33 min. These observations reveal a clear interactive effect between residence time and the W-B ratio on bio-oil production. The contour plot further suggests that balanced, moderate combinations of residence time and W-B ratio are most favorable for obtaining higher bio-oil yields. In addition, the 3D response surface indicates that increasing residence time alongside higher W-B ratios enhances bio-oil formation, in agreement with the findings reported by Akhtar and Amin [18]. Notably, reasonably high bio-oil yields can also be obtained at moderate residence times when paired with relatively high W-B ratios, highlighting the flexibility of these operating parameters for optimizing the hydrothermal carbonization process.

Figure 14 displays the three-dimensional response surface along with the corresponding contour plots that describe the combined effects of the biomass–water (W-B) ratio and heating rate (Hr) on oil yield during hydrothermal carbonization (HTC). The results indicate that, within the studied operating range, both parameters exert only a minor influence on oil production. However, a slight improvement in oil yield is observed as the biomass-water ratio and heating rate increase, suggesting a weak but noticeable positive relationship between these operating conditions and oil yield.

Figure 15 presents the three-dimensional response surface along with the associated contour plots showing how residence time (Rt) and heating rate jointly affect oil yield during the process. The surface reveals a steady, almost linear rise in oil yield as both residence time and heating rate increase. The wide spacing of the contour lines indicates that variations in oil yield across the examined range are relatively modest. This suggests that although longer reaction times and higher heating rates contribute positively to oil production, their influence is moderate rather than decisive, and no distinct optimum is evident within the studied operating conditions.

3.5 Optimization result for production of char

Table 9 outlines the optimization constraints and objective functions established for the independent variables and the response parameters. In this framework, temperature, residence time, and heating rate were assigned maximization goals, while the water-biomass (W-B) ratio was constrained to a minimum. With respect to the response variables, the optimization approach aimed to reduce bio-oil yield while concurrently enhancing char yield, surface area, pore size, and pore volume. The numerical optimization produced a single optimal solution, which is summarized in Table 10 along with the associated operating conditions and predicted response values. From the evaluation of 90 initial starting points, the selected solution achieved a desirability value of 0.498. This desirability score reflects a moderate level of optimization performance, indicating that the identified conditions represent a reasonable balance among the competing objectives of the process parameters and the targeted response outcomes.

Table 9 Optimization constraints

Name	Goal	Lower Limit	Upper Limit	Lower Weight	Upper Weight	Importance
A:Reaction Temperature	maximize	180	220	1	1	3
B:W-B Ratio	minimize	8	12	1	1	3
C:Reaction Time	maximize	30	90	1	1	3
D:Heating Rate	maximize	4	7	1	1	3
Char yield	maximize	23.438	48.612	1	1	3
OIl yield	minimize	19.353	30.72	1	1	3
specific surface area	maximize	175.003	553.488	1	1	3
pore size	maximize	1.24	2.96	1	1	3
pore volume	maximize	0.14	2.9	1	1	3

Table 10 Optimized result of hydrochar experiment for use as adsorbents

S/N	Temperature (^{o} C)	Residence Time (mins)	Heating Rate (^{o} C/mins)	W-B ratio (g)	Char Yield (%)	Oil Yield (%)	Surface area (m2 /g) /g)	Pore size (nm)	Pore volume (cm3
1	203.699	8.000	90.000	6.628	33,856	28.149	433.302	2.311	0.431

The overall desirability of the optimization result is depicted in Fig. 16 through a bar chart. This graphical representation emphasizes the relative influence of the main process parameters used to determine the optimal operating conditions. Taken together, the chart offers useful insight into the key

factors controlling the production of hydrochar with characteristics that are well suited for adsorbent applications.

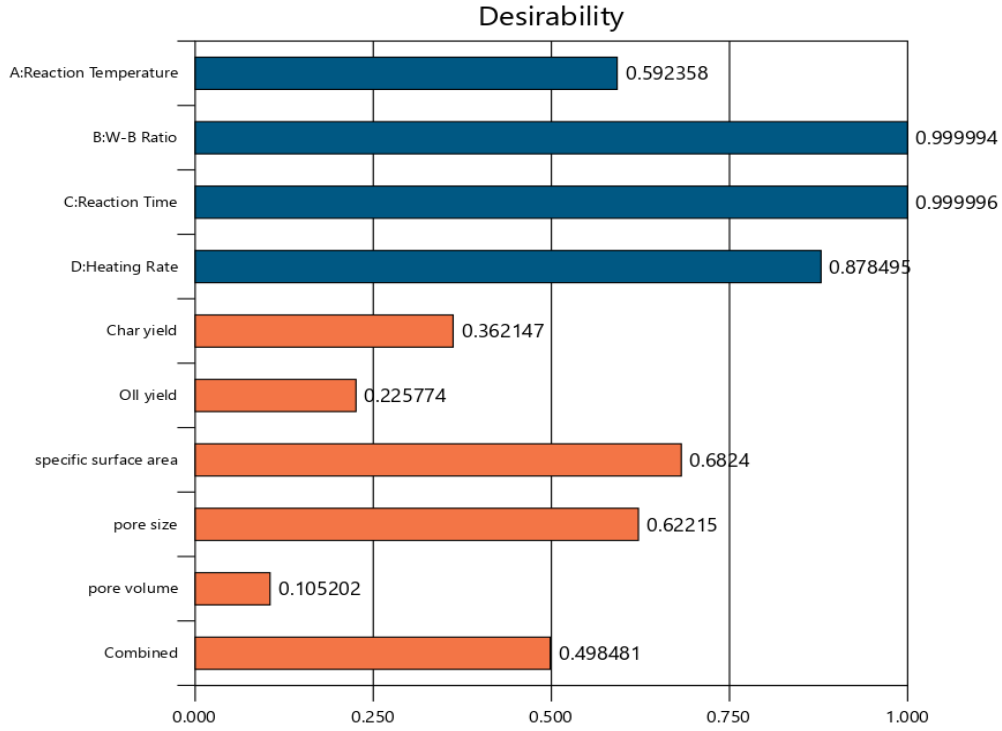


Fig. 16 Bar graph showing desirability

3.6 Post-analysis of results

The results presented in Tables 11 and 12 show a 95% confidence level and 99% population coverage, supporting the reliability and effectiveness of the proposed solution. The accuracy and validity of this optimized solution were further confirmed through analysis using Design-Expert software.

Table 11 Post analysis on factor

Factor	Name	Level	Low Level	High Level	Std. Dev.	Coding
A	Reaction Temperature	200.00	180.00	220.00	0.0000	Actual
B	W-B Ratio	10.00	8.00	12.00	0.0000	Actual
C	Reaction Time	60.00	30.00	90.00	0.0000	Actual
D	Heating Rate	5.50	4.00	7.00	0.0000	Actual

Table 12 Post analysis on factor and point predictions

Analysis	Predicted Mean	Predicted Median	Std Dev	SE Mean	95% CI low for Mean	95% CI high for Mean	95% TI low for 99% Pop	95% TI high for 99% Pop

Char yield	36.627	36.627	1.824	0.442	35.663	37.591	28.718	44.537
OIl yield	26.026	26.026	1.617	0.392	25.171	26.881	19.016	33.037
specific surface area	380.643	380.643	63.465	15.392	347.106	414.181	105.491	655.795
pore size	2.006	2.006	0.341	0.083	1.826	2.186	0.528	3.484
Pore volume	0.366	0.366	0.065	0.016	0.332	0.401	0.087	0.646

3.7 Characterization of AFPN Biomass and Resulting Hydrochar

3.7.1 Comparison of Elemental and Proximate Properties

Ultimate and proximate analyses were performed on the AFPN and AFPNH samples to assess their elemental composition (C, H, N, S, O), H/C and O/C ratios, as well as their proximate properties. The findings are summarized in Table 13 and visually compared in Fig. 17 using a color-coded bar chart for clarity.

3.8 Ultimate analysis

The ultimate analysis provides insight into the elemental composition of the samples by measuring carbon (C), hydrogen (H), nitrogen (N), oxygen (O), and sulfur (S) (CHNOS). The results indicate that AFPNH220 (90 min) has the highest carbon content, whereas the untreated biomass feedstock (AFPN) shows the lowest. This increase in carbon is primarily linked to thermally driven reactions, such as dehydration and polymerization, which occur under elevated hydrothermal carbonization conditions, enhancing biomass conversion and carbon enrichment. Conversely, the oxygen content follows an opposite trend: the raw AFPN sample contains the highest oxygen proportion, which decreases progressively with increasing treatment temperature. This reduction is due to the preferential removal of oxygen-containing functional groups during high-temperature processing, leading to a lower oxygen content and a corresponding relative increase in carbon concentration. Additionally, the H/C and O/C atomic ratios were analyzed to evaluate the degree of carbonization. A higher H/C ratio suggests improved energy efficiency and better fuel quality of the resulting hydrochar.

3.9 Proximate analysis

The proximate analysis results, shown in Table 13 and illustrated in Fig. 17, were assessed alongside the ultimate analysis data. In the figure, each sample is represented by a different color, with the bars indicating moisture content (MC), ash content (AC), volatile matter (VM), and fixed carbon (FC) for each sample. The results reveal that the raw biomass has the highest moisture content, which gradually decreases during the carbonization process. Ash content, on the other hand, steadily increases with rising HTC temperatures. Volatile matter initially rises with temperature but later declines at higher temperatures. This pattern reflects the generation of more volatile compounds as temperature increases and the reduction in carbon loss during HTC, highlighting the process's effectiveness in modifying the material's composition while preserving carbon.

Table 13 Ultimate and proximate analysis of AFPN and the hydrochars

Parameter	Raw AFPN	200 (60 min) AFPNH	220 (90 min) AFPNH
Proximate Analysis (%)			
Moisture content	4.7.0	3.8	3.1
Ash content	10.0	6.2	8.8
Volatile matter	65.0	69.2	61.4
Fixed carbon	17.5	18.7	27.0
Ultimate Analysis			
Carbon	25.73	48.82	52.42
Hydrogen	5.71	3.33	2.42
Nitrogen	9.43	13.32	12.35
Oxygen	61.07	41.56	36.51
Sulphur	0.48	0.02	0.003
H/C	0.22	0.07	0.05
O/C	2.37	0.85	0.70

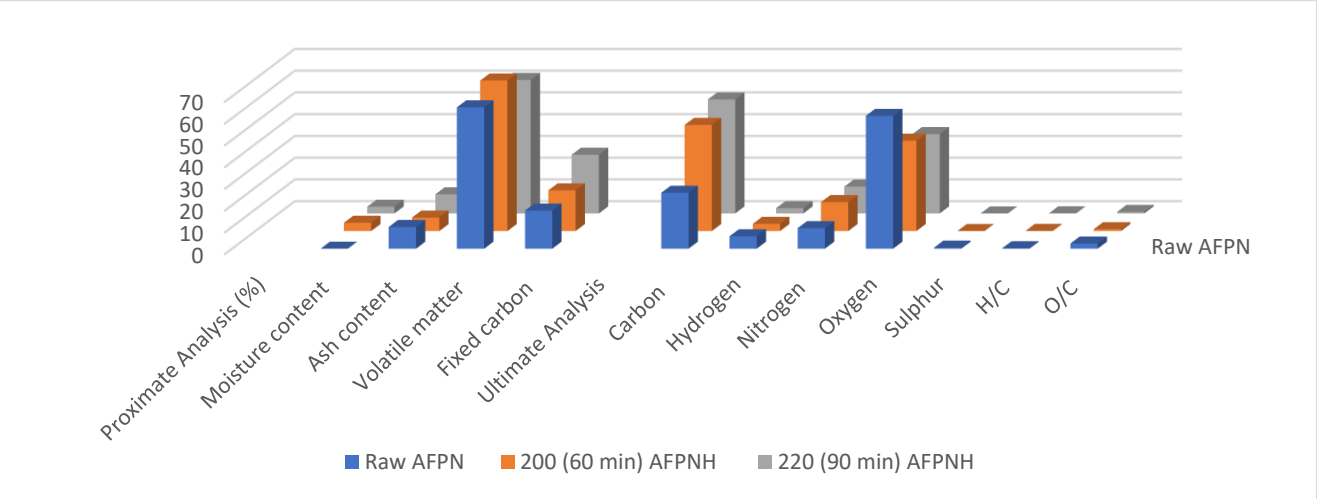
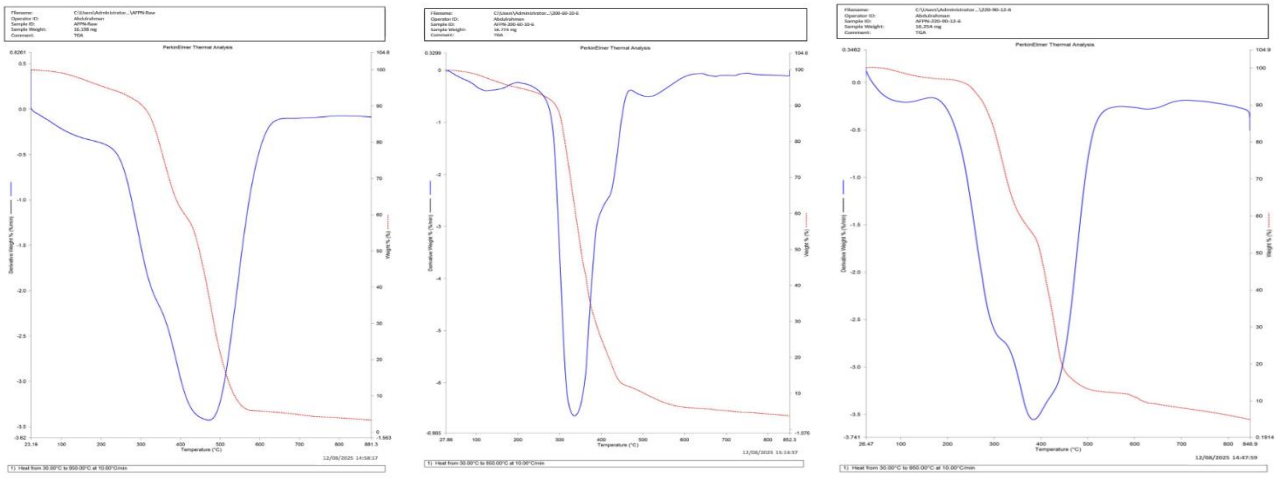


Fig. 17**.** Comparative ultimate and proximate analysis of the biomass feedstock and hydrochar samples.

3.9.1 Thermogravimetric Analysis (TGA)

Figure 18 presents the thermogravimetric analysis (TGA) profiles of the three samples, following ASTM D7582 standards. All samples experienced an initial mass loss below 105 °C, corresponding to moisture contents of roughly 3-5 wt.% with minor differences among them. Volatile matter, defined as the mass loss occurring between 105 and 400 °C under inert conditions, showed a decreasing trend across the samples: 68-70 wt.% in Sample A, 60-63 wt.% in Sample B, and the lowest in Sample C, reflecting the gradual reduction of thermally labile components. In contrast, fixed carbon content, calculated by difference, increased progressively from 18-22 wt.% up to 25-29 wt.%, while ash content, determined from the residual mass at 850-900 °C, rose from 5-7 wt.% to 8-10 wt.%. This pattern demonstrates a clear enrichment in carbon and minerals across the samples, in line with ASTM D7582 criteria.



Raw AFPN AFPNH at 200 °C AFPNH at 220 °C

Figure 18 TGA/DTA curve of the raw, and char sample at 200 °C, and 220 °C,

4. Conclusion

This study highlights African Fan Palm Nut as a highly promising feedstock for producing hydrochar through hydrothermal carbonization (HTC). The findings show that key operational parameters temperature, biomass-to-water ratio, reaction time, and heating rate have a significant impact on both the yield and quality of the hydrochar. Under optimized conditions of 203.7 °C, a biomass-to-water ratio of 1:8, a residence time of 90 min, and a heating rate of 6.63 °C/min, the process achieved a dry yield of 33.86%, an oil yield of 28.15%, a specific surface area of 433.3 m^2/g, pore size of 2.31 nm, and pore volume of 0.431 cm^3. The resulting hydrochar demonstrated enhanced physicochemical properties, including increased carbon content (27.0%), reduced ash content (8.8%), and greater stability due to lower volatile matter. These characteristics make it suitable for a variety of environmental and agricultural applications. Specifically, its low ash content and high surface area make it an effective soil amendment and a capable adsorbent for wastewater treatment, including the removal of heavy metals and organic dyes. Additionally, the high carbon content and stability suggest potential applications in carbon sequestration and energy production. On the whole, this work underscores the value of converting agricultural residues like African Fan Palm Nut into functional carbon-based materials, addressing waste management challenges while promoting sustainable energy solutions. By valorizing biomass waste, the study contributes to renewable energy development and supports a circular economy approach. Future research should explore process scale-up, long-term effects on soil, and practical performance evaluations in applications such as adsorption, filtration, and energy generation.

Acknowledgements: The authors sincerely acknowledge the Department of Mechanical Engineering, Nnamdi Azikiwe University, Awka, Nigeria, for providing the laboratory facilities used in conducting this research. The authors also appreciate the technical support provided by laboratory staff during the experimental work.

Author Contributions: All authors actively contributed to the development and design of the study. The first author carried out the experiments and performed the data analysis. The second author supported the study's conceptualization, assisted with data interpretation, and helped prepare the

manuscript. The third and fourth authors provided critical revisions of the manuscript and gave approval for the final version.

Funding: The authors state that this manuscript was prepared without any financial support, grants, or funding from external sources.

Data Availability: The authors confirm that no funding, grants, or financial support were received for this study. The datasets produced and/or analyzed during the research can be obtained from the corresponding author upon reasonable request.

Declarations

Conflict of Interest: The authors confirm that they have no conflicts of interest to disclose.

References

1. Ahmad F, Silva EL, Varesche MBA (2018) Hydrothermal processing of biomass for anaerobic digestion – A review. Renew Sustain Energy Rev 98:108–124. https://doi.org/10.1016/j.rser.2018.09. 008
2. Ezenwa ON, Mgbemena CO, Emagbetere E (2023) Design and Construction of a Continous Stirring Hydrothermal Liquefaction Batch Reactor. Tuijin Jishu/J Propuls Technol. 44(3):2021–2032
3. Ezenwa ON, Mgbemena CO, Emagbetere E (2024) Utilization of solid residue from hydrothermal liquefaction of breadfruit pulp for the production of bio-briquette using cassava starch as binder. Heliyon 10(1):e24081. https://doi.org/10.1016/j.heliyon.2024. e24081
4. Manyà JJ, García-Morcate D, González B (2020) Adsorption performance of physically activated biochars for postcombustion Co2 capture from dry and humid fue gas. Appl Sci. https://doi.org/10. 3390/APP10010376
5. Khosravi A, Zheng H, Liu Q, Hashemi M, Tang Y, Xing B (2022) Production and characterization of hydrochars and their application in soil improvement and environmental remediation. Chem Eng J. https://doi.org/10.1016/J.CEJ.2021.133142
6. Jha S, Gaur R, Shahabuddin S, Tyagi I (2023) Biochar as Sustainable Alternative and Green Adsorbent for the Remediation of Noxious Pollutants: A Comprehensive Review. Toxics 11(2):1–23. https://doi.org/10.3390/toxics11020117
7. Jaruwat D, Udomsap P, Chollacoop N, Fuji M, Eiad-Ua A (2018) Efects of hydrothermal temperature and time of hydrochar from Cattail leaves. AIP Conf Proc. https://doi.org/10.1063/1.5053192
8. Belaud JP, Prioux N, Vialle C, Sablayrolles C (2019) Big data for agri-food 4.0: Application to sustainability management for by-products supply chain. Comput Ind 111:41–50. https://doi.org/10.1016/j.compind.2019.06.006
9. Gaibor-Chávez J, Pérez-Pacheco S, Velázquez-Martí B, Niño-Ruiz Z, Domínguez-Narváez V (2016) Dendrometric characterization of corn cane residues and drying models in natural conditions in Bolivar Province (Ecuador). Renew Energy 86:745–750. https://doi.org/10.1016/j.renene.2015.09.009

10. Yusuf I, Flagiello F, Ward NI, Arellano-García H, AvignoneRossa C, Felipe-Sotelo M (2020) Valorisation of banana peels by hydrothermal carbonisation: Potential use of the hydrochar and liquid by-product for water purifcation and energy conversion. Bioresour Technol Reports. https://doi.org/10.1016/J.BITEB. 2020.100582
11. Devnath B, Khanal S, Shah A, Reza T (2024) Infuence of Hydrothermal Carbonization (HTC) Temperature on Hydrochar and Process Liquid for Poultry, Swine, and Dairy Manure. Environ - MDPI. https://doi.org/10.3390/ENVIRONMENTS11070150
12. United Nations. (2020). *The Sustainable Development Goals Report 2020*. United Nations. https://sdgs.un.org
13. Cao Y, He M, Dutta S, Luo G, Zhang S, Tsang DCW (2021) Hydrothermal carbonization and liquefaction for sustainable production of hydrochar and aromatics. Renew Sustain Energy Rev. https://doi.org/10.1016/J.RSER.2021.111722
14. Orisa CA, Amadi AO, Onyechege IC, Owunna RN (2024) "Proximate Composition, Storage Stability, and Sensory Properties of Table Spread Produced from African Elemi (Canarium schweinfurthii)", IPS Appl. J Nutr Food Metab Sci 2(1):27–33. https://doi. org/10.54117/IAJNFMS.V2I1.56
15. Ndukwu MC, Ehiem J, Mbanasor J, Obasi N (2022) Thermal softening kinetics of African black olive fruit: Infuence of temperature and water absorption on the thermal maceration dynamics and thermophysical properties. J Food Process Preserv. https:// doi.org/10.1111/JFPP.17021
16. Titiladunayo RA, Akinnuli IF, Lukman BO, Ikubanni AF, Agboola P (2018) Modelling the Energy Content of Municipal Solid Waste and Determination of its Physicochemical Correlation, Using Multiple Regression Analysis. Int. J. Mech. Eng. Technol. 9:220–232
17. Calistus P. Odeh, Chinedum O. Mgbemena Benjamin U. Oreko, (2025) Impact of processing parameters on the hydrothermal carbonisation of African Elemi Shell J. Umm Al-Qura Univ. Eng.Archit. https://doi.org/10.1007/s43995-025-00135-y
18. Kambo HS, Dutta A (2015) A comparative review of biochar and hydrochar in terms of production, physico-chemical properties and applications. Renew Sustain Energy Rev 45:359–378. https://doi. org/10.1016/J.RSER.2015.01.050
19. Qureshi KM, Kay Lup AN, Khan S, Abnisa F, Wan Daud WMA (2021) Optimization of palm shell pyrolysis parameters in helical screw fuidized bed reactor Efect of particle size pyrolysis time and vapor residence time. Clean Eng Technol. https://doi.org/10. 1016/j.clet.2021.100174
20. Akhtar J, Amin NAS (2011) A review on process conditions for optimum bio-oil yield in hydrothermal liquefaction of biomass. Renew Sustain Energy Rev 15(3):1615–1624. https://doi.org/10. 1016/j.rser.2010.11.054

Supplementary Files

This is a list of supplementary files associated with this preprint. Click to download.

- GraphRepHydrothermalcarb.jpg